Drag Reduction Using Riblet Film Applied to Airfoils for Wind Turbines

Agrim Sareen
e-mail: sareen2@illinois.edu

Robert W. Deters
e-mail: rdeters@illinois.edu

Steven P. Henry
e-mail: henry12@illinois.edu

Michael S. Selig
Associate Professor
e-mail: m-selig@illinois.edu

Department of Aerospace Engineering,
University of Illinois at Urbana-Champaign,
Urbana, IL 61801

This paper presents results of a study that was commissioned by the 3M Renewable Energy Division to measure the drag reduction by using riblet film on airfoils specifically designed for wind turbine applications. The DU 96-W-180 airfoil was tested with four different symmetrical V-shaped riblet sizes (44, 62, 100, and 150-μm) at three Reynolds numbers (1×10^6, 1.5×10^6, and 1.85×10^6) and at angles of attack spanning the low drag range of the airfoil. Tests were run with riblet film covering different sections of the airfoil in order to determine the optimal riblet location in terms of drag reduction. Results showed that the magnitude of drag reduction depended on the angle of attack, Reynolds number, riblet size, and riblet location. For some configurations, riblets produced significant drag reduction of up to 5%, while for others riblets were detrimental. Trends in the results indicated an optimum riblet size of 62-μm for the range of Reynolds numbers at which tests were conducted. The airfoil chord was 18 in (0.457 m). Results also showed that each riblet size performed best at a given Reynolds number with the optimal Reynolds number decreasing with an increase in riblet size.
[DOI: 10.1115/1.4024982]

1 Introduction

Riblets have been known to reduce skin friction drag for the past 30 years. 3 M has been pioneering the development of riblet film technology since the early 1980 s and has provided experimental riblet film to many research centers to study the aerodynamic performance of riblets. Despite the ongoing research on riblets, challenges such as finding the optimal riblet size and placement for airfoil drag reduction still remain. A majority of the research done on riblet film has been on turbulent flat plates. Moreover, recent research on airfoils has been incomplete with many such studies producing more questions than answers. Most past efforts to study riblets have aimed at validating the drag reducing properties of riblets as opposed to finding the optimal riblet configuration for drag reduction. Riblets have often been placed covering almost the entire airfoil surface by forcing transition ahead of the film. While this approach might be conducive to studying the drag reducing properties of riblets, it does not address how riblets might perform in a real world application such as on wind turbine blades where flow remains laminar until natural transition.

Dr. Robert L. Ash [1] from the Old Dominion University started the ideas related to riblet film. Early research by Walsh [2] reported a drag reduction of 4–7% using riblets on turbulent flat plates. Subsequent research observed skin friction drag reduction of the same magnitude in turbulent boundary layers [3–5]. A few years after these initial reports, Bechert et al. [6] published a paper relating "ribs" on shark skin to riblet film. In more recent studies, Savill [7] discussed the application of riblets to wind turbines and aircraft.

Most early research dealing with riblets was done on flat plates; however, due to the difference in boundary-layer characteristics of flat plates and airfoils, recent studies have focused on the application of riblet film to airfoils. A commonly tested airfoil has been the NACA 0012, which is often used for academic research. Caram and Ahmed [8,9] tested three riblet sizes (23, 76, and 152-μm) on the NACA 0012 at Re = 250,000 and observed a drag reduction of 13% with the 152-μm riblets. However, this study was done at just one angle of attack (0 deg) and with the flow tripped near the leading edge at $x/c = 10\%$. Han [10] tested the same airfoil with 180-μm riblets covering the entire airfoil at a much lower Reynolds number of 17,000 and 36,000 and reported a drag reduction of around 4% and 16% respectively. The drag reduction observed in this case, however, could have been due to a reduction in the size of the laminar separation bubble caused by the film as opposed the action of riblets. In another study, Sundaram et al. [11] tested the NACA 0012 with 76 and 152-μm riblets applied at $x/c = 12$–96% and trips at $x/c = 10\%$. Tests were run at angles of attack ranging from 0 to 6 deg and $Re = 1{,}000{,}000$. A maximum drag reduction of 13% was reported for the 152-μm riblets at 6 deg.

In a similar study, the GAW-2 and LC100D airfoils were tested with the 76 and 152-μm riblets [12–14]. Similar to the NACA 0012 airfoil, the GAW-2 airfoil showed a maximum drag reduction of 14% with 152-μm riblets at 6 deg and Re = 1,000,000. Riblets on the LC100D airfoil, however, were not as effective with a maximum drag reduction of only 2% at Re = 500,000. Studies on other airfoils and riblet sizes have reported drag reduction in the range of 6–12% with similar trends [15,16].

As mentioned previously, most of these studies were limited to the validation of the drag reducing properties of riblets in turbulent boundary layer and were therefore conducted by tripping the flow near the leading edge, applying riblets in the resulting turbulent region, and comparing the drag before and after the application of riblets. Riblets have never been tested with the film applied downstream of the natural transition point. Additionally, tests have been performed at selected angles of attack and Reynolds numbers. No real effort has been made to perform a comprehensive study, testing riblets over the entire drag polar and multiple Reynolds numbers, with the aim of optimizing them for real world applications such as wind turbines. The goal of this research was to test riblet film on a wind turbine airfoil by varying the riblet size and location over a range of angles of attack and Reynolds numbers. Results should help improve the understanding of riblet performance, expose trends in riblet effectiveness with size and location, and thereby help determine the

Contributed by the Solar Energy Division of ASME for publication in the Journal of Solar Energy Engineering. Manuscript received November 7, 2011; final manuscript received June 16, 2013; published online September 16, 2013. Assoc. Editor: Christian Masson.

optimal riblet configurations for application to wind turbine blades for increased energy capture.

2 Approach and Experimental Methods

The critical factor to be considered while testing riblets is the riblet film placement. Wind turbine airfoils, such as the one used for this study, can have a laminar separation bubble that lies between the laminar and turbulent flow regions. Placing the riblet film near the leading edge (where the flow is laminar) might result in lower drag; however, this change might not be due to the action of the riblets but due to the change in location of the transition point and consequently, a change in the length of the laminar separation bubble. Hence, in order to determine the riblet placement that would maximize the benefit while ensuring that any drag reduction measured would be due solely to the riblets, a preliminary computational analysis was performed on the airfoil followed by wind tunnel flow visualization. The results from this analysis and flow visualization are discussed in this section along with the experimental methods, riblet film, and airfoil used for the tests.

2.1 Wind Tunnel Facility. Testing was conducted in the UIUC low-turbulence subsonic wind tunnel. Figure 1 shows the schematic of the tunnel. The wind tunnel is an open-return type with a 7.5:1 contraction ratio. The rectangular test section is 2.8×4.0 ft (0.853×1.219 m) in cross section and 8-ft (2.438-m) long. Over the length of the test section, the width increases by approximately 0.5 in. (1.27 cm) to account for boundary-layer growth along the tunnel side walls. Test-section speeds are variable up to 160 mph (71.53 m/s) via a 125-hp (93.25-kW) alternating-current electric motor driving a five-bladed fan. The tunnel settling chamber contains a 4-in. (10.16-cm) thick honeycomb and four antiturbulence screens. The maximum Reynolds number that can be reached is 1.5×10^6/ft (4.92×10^6/m). The turbulence intensity has been measured to be less than 0.1% [17].

The airspeed and dynamic pressure in the test section were determined by static pressure measurements in the wind tunnel contraction. Ambient pressure was measured with an absolute pressure transducer. Ambient temperature was measured with a thermocouple. The performance of the airfoil was measured using a three-component external force and moment balance mounted underneath the test section and by a wake rake. The model was mounted with the spanwise axis in the vertical direction.

The three-component balance measured the normal force, axial force, and the pitching moment of the airfoil. Lift and drag were calculated from the normal and axial forces, but a more accurate drag value was determined from wake rake measurements. The rake contained 59 total pressure probes over a total width of 9.75 in (24.77 cm). The seven probes on each of the outer sides of the rake were spaced 0.27-in. (6.86-mm) apart and the rest of the 45 probes were spaced 0.135-in. (3.43-mm) apart. Eight spanwise wake profiles were measured for each angle of attack starting 4-in. (10.16-cm) above and ending 3-in. (7.62-cm) below center span, and the resulting drag values were averaged. Only wake rake drag measurements are reported in this paper.

All measurements were corrected for wind tunnel effects and validated by comparing data taken for an S809 airfoil model with data taken at Delft and The Ohio State University [18]. The uncertainty of the measurements was determined to be less than 0.1% in a previous analysis [17].

2.2 Riblet Film. The riblet films tested were manufactured by the 3 M Renewable Energy Division Laboratory. The films tested were off-the-shelf experimental samples, manufactured solely for the purpose of the research and are not commercially available. The films had a plastic backing with V-shaped riblets on one side and an adhesive on the other. Four riblet film samples having riblet heights of 44, 62, 100, and 150 μm were tested. The riblet geometry was manufactured such that the peak-to-valley height and peak-to-peak spacing was the same. Figure 2(*a*) shows an image of the 44-μm riblet film taken using a scanning electron microscope. A similar image of the riblet profile of the 62-μm film is shown in Fig. 2(*b*). The riblet sizes were selected based on the theoretical optimal riblet heights (h) for the Reynolds number range at which testing was done and were calculated using the following equation:

$$h = \frac{(h+)\nu}{U_\infty \sqrt{C_{fx}/2}} \tag{1}$$

where $h+$ is the nondimensional riblet height, ν is the kinematic viscosity and C_{fx} is the local skin friction coefficient at a point on the airfoil [19]. The C_{fx} values were obtained from XFOIL [20].

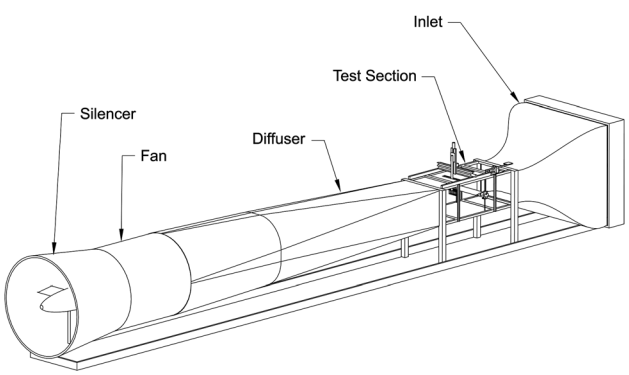

Fig. 1 Schematic of the UIUC low-turbulence subsonic wind tunnel

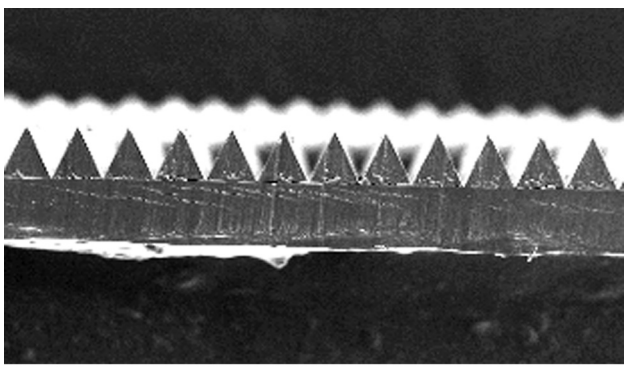

(a)

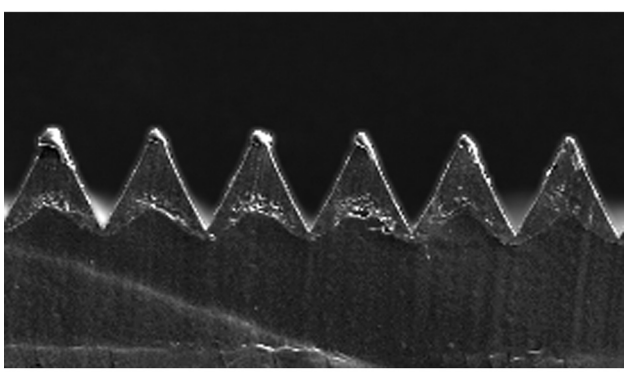

(b)

Fig. 2 Riblet film viewed under a scanning electron microscope: *a*) 44-μm riblet film, and *b*) 62-μm riblet film (courtesy of 3 M)

The h value at each location on the airfoil was weighted using the local skin friction drag at that location normalized by the total drag. The calculated h values were then averaged to get the optimal riblet height for the Reynolds numbers at which tests were conducted. The optimal riblet height was calculated to be 80-μm.

2.3 Airfoil Model. With wind turbines being the primary application for riblet film in this study, the DU 96-W-180 airfoil was chosen for the tests. The DU 96-W-180 is an 18%-thick airfoil designed at Delft University [21]. It was designed to be used at the 75% blade station and is actively used in wind energy research and found in literature. The airfoil model had a span of 33.5-in. (0.851-m) with an 18-in. (0.457-m) chord.

2.4 Viscous Analysis. Before testing the airfoil with film applied to it, the airfoil was analyzed to determine the expected performance for clean and tripped conditions. The airfoil analysis was performed using XFOIL [20], which is capable of modeling

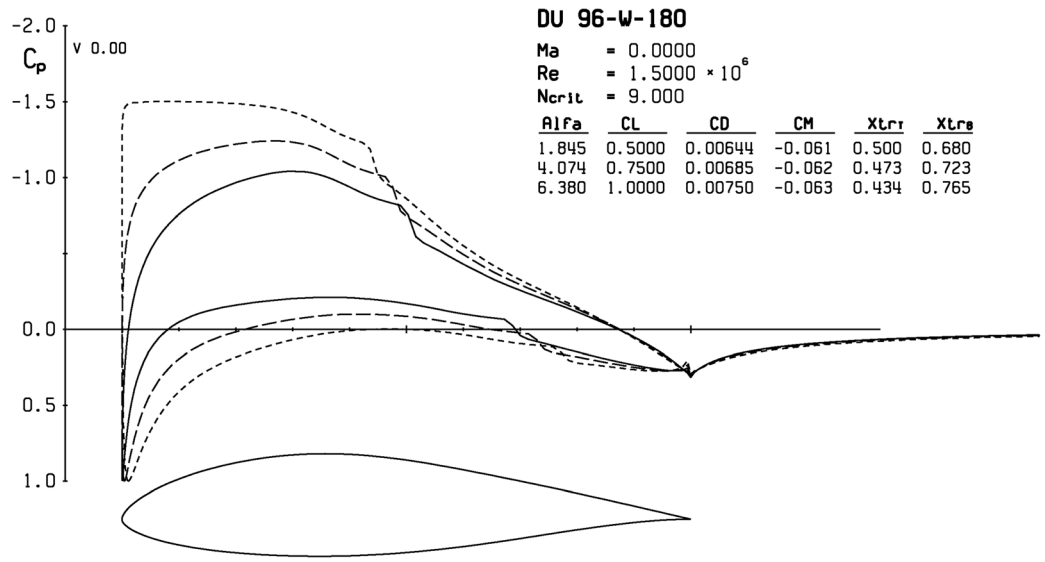

Fig. 3 C_p distribution for the DU 96-W-180 at Re = 1,500,000 as predicted by XFOIL

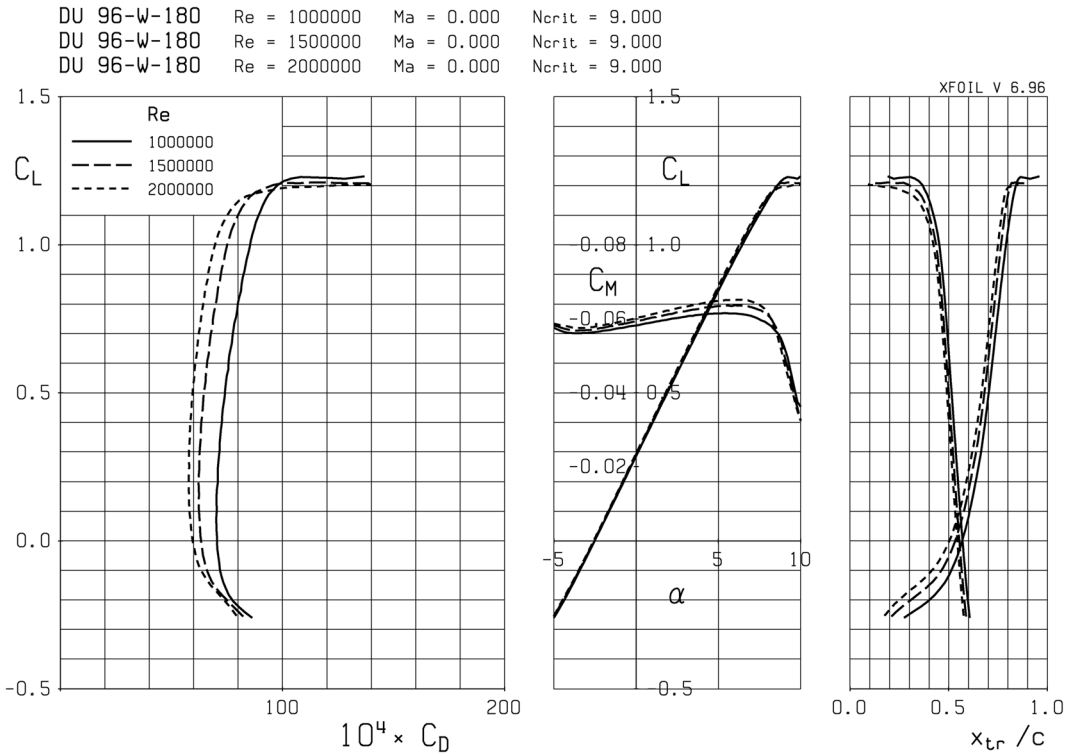

Fig. 4 Drag polar for the DU 96-W-180 at Re = 1,500,000 as predicted by XFOIL

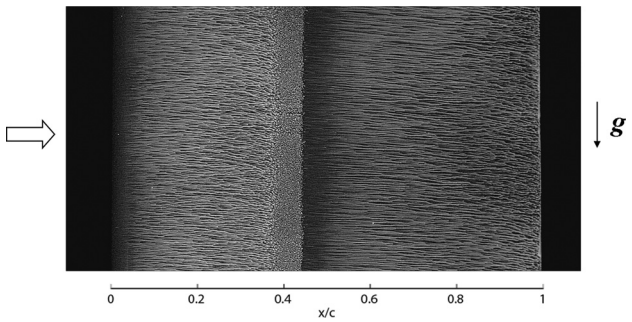

Fig. 5 Flow visualization on the upper surface of the DU 96-W-180 airfoil at $\alpha = 6$ deg and Re = 1,500,000

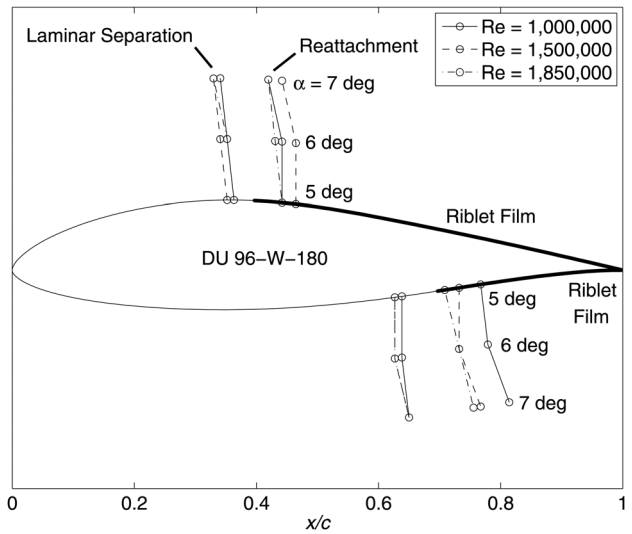

Fig. 6 Laminar separation, reattachment and riblet film locations on the DU 96-W-180 airfoil at angles of attack near maximum *L/D* (symbols correspond to *x/c* locations and not airfoil surface normal)

the effects of laminar separation bubbles. The analysis was performed at Reynolds numbers of 1,000,000, 1,500,000, and 2,000,000 corresponding to the wind tunnel test conditions. The primary reason behind this analysis was to understand the behavior of the clean airfoil. A second reason was to ascertain whether or not the airfoil performance might be improved if the riblet film acted in such a way as to promote transition and thereby reduce the drag of the laminar separation which could inadvertently and incorrectly be attributed to riblet film drag reduction. This question was addressed by analyzing the airfoil with transition fixed at various increments ahead of the laminar separation point.

Figures 3 and 4 show the predicted pressure distributions and drag polars for the DU 96-W-180 airfoil. The polar shows that the low drag range for the DU 96-W-180 airfoil ends at a C_l of approximately 1.2. The pressure coefficient plot (Fig. 3) shows the presence of a laminar separation bubble on both the upper and lower surfaces of the airfoil. It can also be seen in the graphics that natural transition takes place near 40% chord on the upper surface and 75% chord on the lower surface. As discussed previously, placing the riblet film ahead of this laminar separation bubble might produce drag reduction on account of reducing the size of the bubble. In order to avoid tripping the flow (reducing the drag of the bubble) while maximizing the benefit of riblets, the riblet film would need to be positioned to cover only the turbulent region with the front edge of riblet film starting inside the laminar separation bubble and never extending in front of laminar separation point. This primary configuration should prevent the riblet film from influencing transition and shortening the laminar separation bubble, thereby preventing misleading results.

2.5 Surface Oil-Flow Visualization. In addition to the viscous analysis, flow visualization was performed to reveal the exact location and size of the laminar separation bubble on the airfoil model. The process involved spraying the airfoil surface with mineral oil mixed with a florescent pigment, running the tunnel at the desired Reynolds number and observing the flow features under a black light. Flow visualization was performed on the upper and lower surfaces of the airfoil, at the three Reynolds numbers, over the entire low drag range. Figure 5 shows oil-flow visualization on the upper surface of the DU 96-W-180 airfoil at

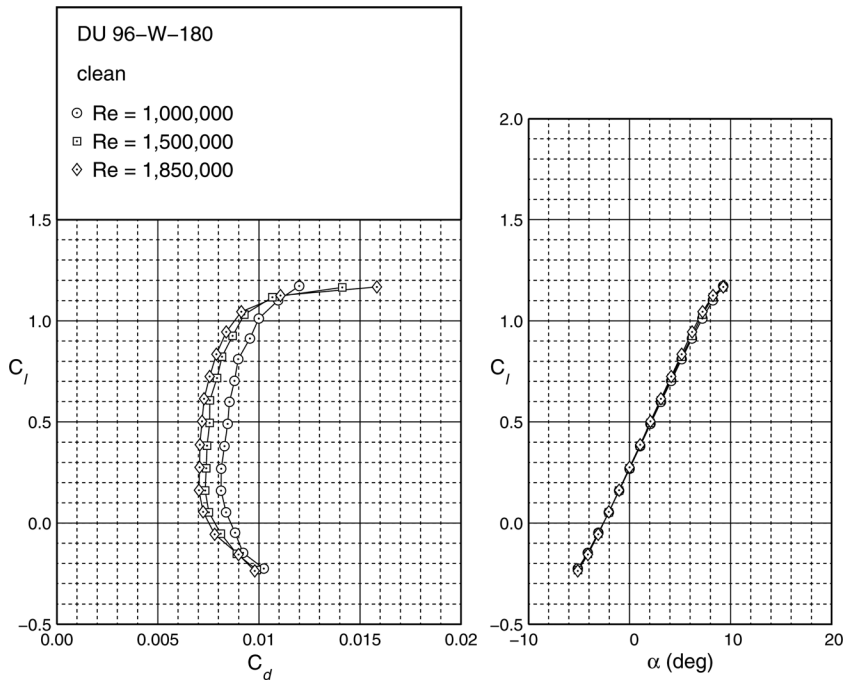

Fig. 7 Drag polars for the clean DU 96-W-180 at the three Re

Re = 1,500,000 and an angle of attack of 6 deg. The image clearly shows a laminar separation bubble starting at 38% chord and reattachment at 45% chord. Consequently, riblet film in the turbulent region would need to be applied starting inside this bubble in order to eliminate the possibility of the leading edge of the film tripping the flow while maximizing the turbulent-region riblet-film coverage for maximum effect.

To determine the approximate location of the film on the airfoil, flow visualization results were examined to determine the location of the laminar separation bubble at various angles of attack. Figure 6 shows the position of the laminar separation and reattachment points at the angles of attack at which the airfoil would most likely be operated (near maximum *L/D*) on a variable-speed wind turbine. The figure also shows the location of the riblet film on the upper surface ($x/c = 40\%$) and lower surface ($x/c = 70\%$). Since the bubble moved with angle of attack, this location would ensure that the riblet film remained inside the bubble for these angles of attack.

2.6 Test Plan. Testing of the riblet film was done by varying both the riblet size and location at Reynolds numbers of 1,000,000, 1,500,000 and 1,850,000. Each configuration was tested over the entire low drag range of the airfoil and each case was run three times to check for repeatability.

Before testing the airfoil with any film on it, the clean airfoil was tested to obtain the baseline drag at the three Reynolds numbers for comparison. Next, the airfoil was tested with trips ahead of the laminar separation point to determine if there was an optimal location that minimized the drag of the laminar separation bubble. The flow was tripped by using a backward facing step created by applying a strip of 0.0045-in. (0.114-mm) thick and 5/16-in. (7.938-mm) wide Chartpack® tape at the desired location. No trips were used when riblet film was later applied.

Based on the fact that the majority of the skin friction drag is due to turbulent flow and the possibility of riblets in the laminar region forcing early transition, it was decided to test riblets only in the turbulent regions (starting inside the bubble so as not to promote transition). The airfoil was tested with riblet film applied to the upper surface turbulent region, lower surface turbulent region, and both upper and lower turbulent regions. When riblet film was placed in the turbulent regions, a narrow piece of tape was used to secure the leading edge of the film to the airfoil and prevent it from debonding (special, removable, low-tack adhesive was used for the films in this research). As mentioned previously, trips were not placed ahead of the riblet film as no benefit to the airfoil performance was observed by eliminating the separation bubble at the Reynolds numbers tested.

3 Results and Discussion

This section discusses the results from the testing of the riblet film on the DU 96-W-180 airfoil at the three Reynolds numbers. As mentioned previously, the airfoil was tested with riblet film applied to the turbulent regions only, prior to which the clean airfoil was tested in order to establish a baseline for drag reduction measurement.

3.1 Clean Airfoil. Before testing the DU 96-W-180 airfoil with riblet film, a baseline was determined against which the effect of riblet film would be compared. Figure 7 shows the performance of the DU 96-W-180 airfoil without trips or riblet film applied at the three Reynolds numbers. This dataset provided the baseline used to measure drag reduction. Tests were also run with trips located near the laminar separation point to check for the possibility of a drag decrement on account of elimination or mitigation of the laminar separation bubble. No benefit, however, was seen from forcing transition ahead of the bubble and in some cases trips even proved to be detrimental to the airfoil performance. Thus, if care was not taken in placing the riblet film behind the natural laminar separation point, misleading results showing drag increase could be observed on account of early transition due to the film.

3.2 Riblets in the Turbulent Region. For each riblet size, tests were run with riblets on the upper surface, lower surface, and both upper and lower surface turbulent regions at the three Reynolds numbers. The results are presented in the form of plots showing drag polars for each case (Figs. 8–19). The plots also show the percent change in drag due to the riblets (negative indicating favorable drag reduction). The percent change in drag was calculated by using the clean case as the baseline.

In general, the riblets on the upper surface (suction side) had a greater impact on the airfoil drag than riblets on the lower surface (pressure side). Maximum drag reduction was obtained with riblets on both the upper and lower surfaces. As mentioned earlier, riblet film was placed based on the location of the laminar separation bubble at angles of attack at which this airfoil would most likely be operated ($C_l = 0.75$–1). Since at C_l values outside this range riblets would no longer start inside the separation bubble, any measured change in drag may not be due to the action of riblets but instead due to early flow transition. Therefore, the assessment of riblet performance will be made based on the drag at C_l values ranging from 0.75 to 1.0.

Figures 8–11 show the drag polars for the four different riblet films applied to the upper surface turbulent region, lower surface turbulent region, and both upper and lower surface turbulent regions compared to the clean airfoil at Re = 1,000,000. It can be seen from the figures that there was a marginal decrease in drag when the 44-μm riblets were used. Both the 62-μm and 100-μm riblets produced a 2–4% reduction in drag with riblets on the upper and lower surfaces. In contrast to the other three riblet sizes, the 150-μm riblets were detrimental, causing an increase in drag.

Figures 12–15 show the drag polars for the four riblet films at $Re = 1{,}500{,}000$. It can be seen from the plots that there was a 1–2% decrease in drag with 44-μm riblets. The 62-μm riblets performed much better producing a drag reduction of 4–5%. The performance of the 100-μm riblets was between the 44 and 62-μm riblets with a drag reduction of 2–4%. The 150-μm riblets were again detrimental causing an increase in drag of up to 6%.

Figures 16–19 show the drag polars for the four riblet films at Re = 1,850,000. At this Reynolds number, the 44-μm riblets had almost no effect, while the 62-μm riblets produced a drag reduction of 1–2%. Both the 100 and 150-μm riblets were highly detrimental to the airfoil performance producing a large increase in drag.

The drag polars show that the performance of riblets is highly dependent on both the riblet size and Reynolds number. Figure 20 shows the measured percent change in drag for each riblet size, with riblets applied to the upper and lower surface turbulent regions of the DU 96-W-180 airfoil. The ΔC_d values have been plotted for three lift coefficients in the range where the airfoil would most likely be operated. Broken lines are used to connect the 44, 62, and 100-μm riblets as different thickness backings were used for the three. The 100 and 150-μm riblets, which had the same backing, are connected by a solid line. The plot clearly shows that there exists an optimum riblet size (62-μm) which is the most effective in reducing drag over the range of Reynolds numbers tested. A decrease or increase in riblet size from the optimum resulted in a reduction in riblet performance.

Figure 21 shows a similar comparison of the four riblet sizes at the three Reynolds numbers and $C_l = 0.75$. The plot illustrates the effect of Reynolds number on the riblet effectiveness. It can be seen that the 62-μm riblet performs the best at all three Reynolds numbers. Comparing the percent change in drag due to each riblet size, it can be seen that the 44 and 62-μm riblets perform best at Re = 1,500,000 while the 100 and 150-μm riblets perform best at $Re = 1{,}000{,}000$. Thus, it can be seen that the optimal Reynolds number for a given riblet size decreases as the riblet size increases.

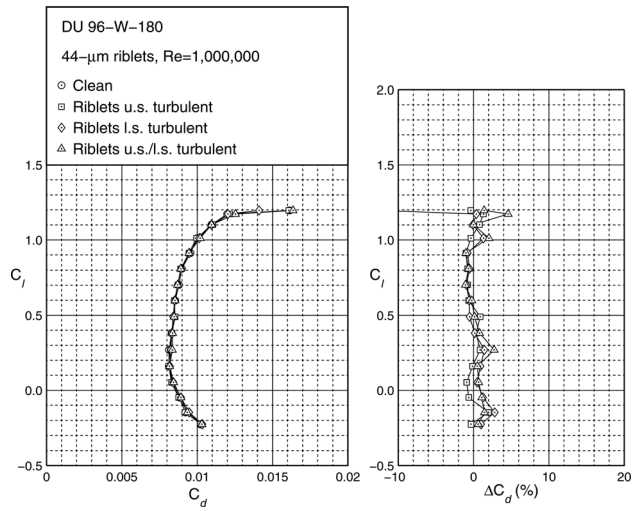

Fig. 8 Drag polar for the DU 96-W-180 at Re = 1,000,000 with 44-μm riblets in the turbulent regions

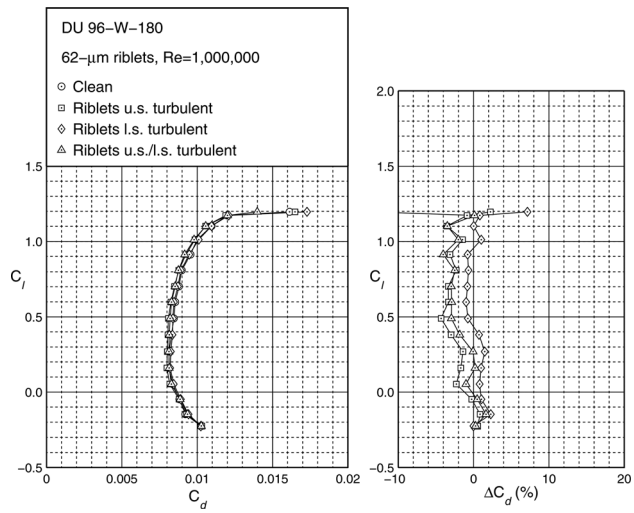

Fig. 9 Drag polar for the DU 96-W-180 at Re = 1,000,000 with 62-μm riblets in the turbulent regions

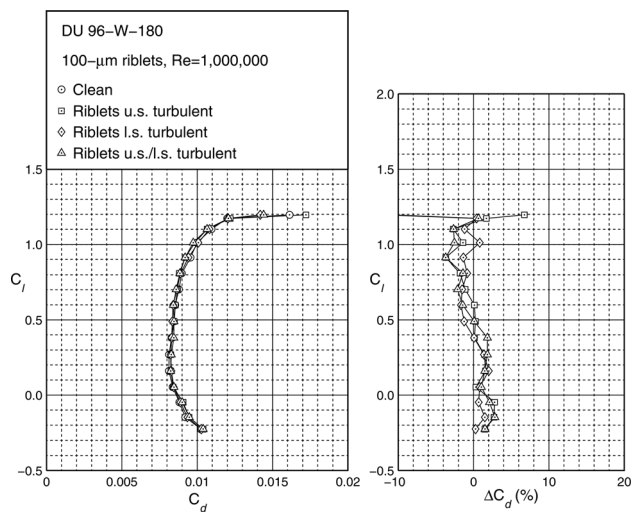

Fig. 10 Drag polar for the DU 96-W-180 at Re = 1,000,000 with 100-μm riblets in the turbulent regions

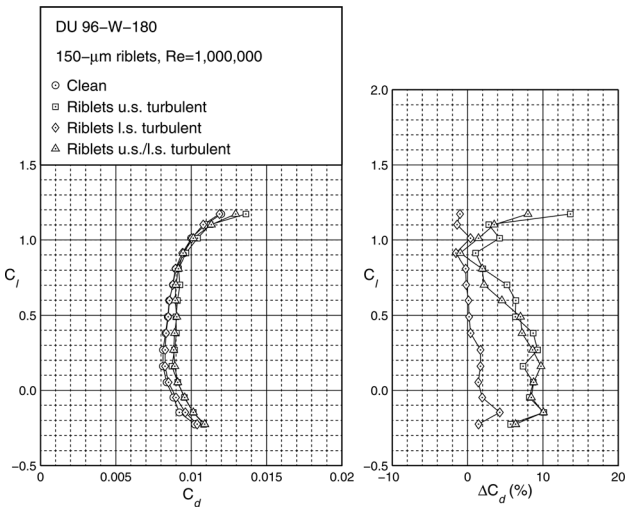

Fig. 11 Drag polar for the DU 96-W-180 at Re = 1,000,000 with 150-μm riblets in the turbulent regions

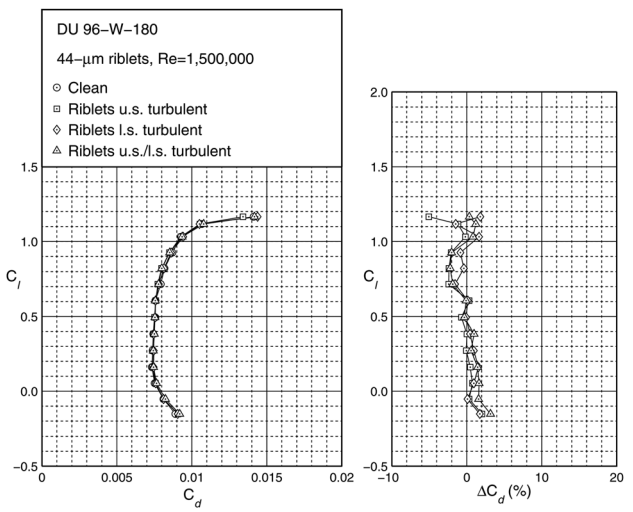

Fig. 12 Drag polar for the DU 96-W-180 at Re = 1,500,000 with 44-μm riblets in the turbulent regions

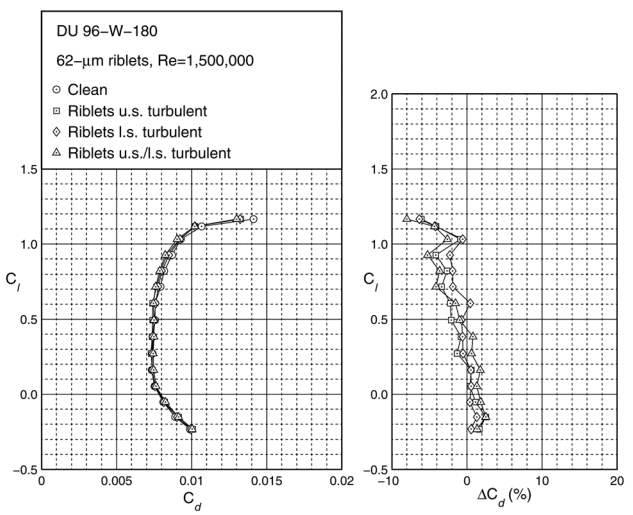

Fig. 13 Drag polar for the DU 96-W-180 at Re = 1,500,000 with 62-μm riblets in the turbulent regions

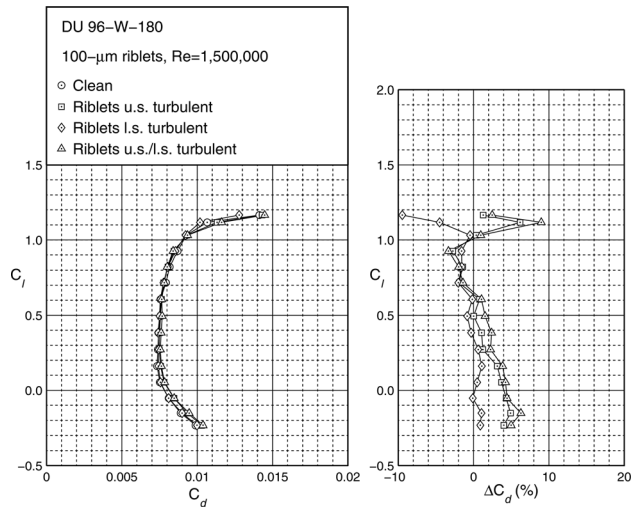

Fig. 14 Drag polar for the DU 96-W-180 at Re = 1,500,000 with 100-μm riblets in the turbulent regions

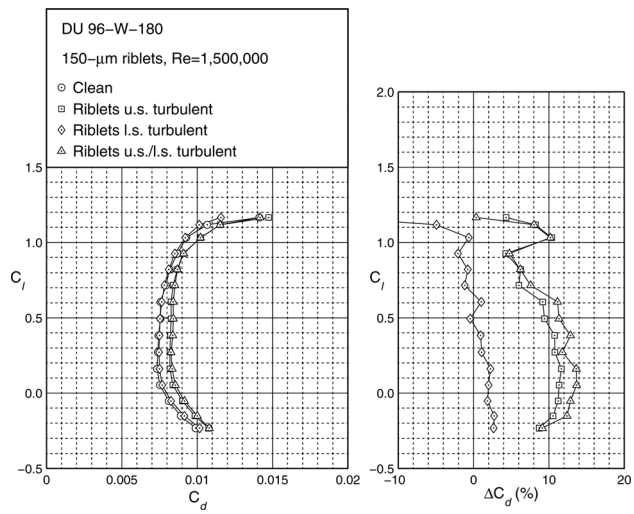

Fig. 15 Drag polar for the DU 96-W-180 at Re = 1,500,000 with 150-μm riblets in the turbulent regions

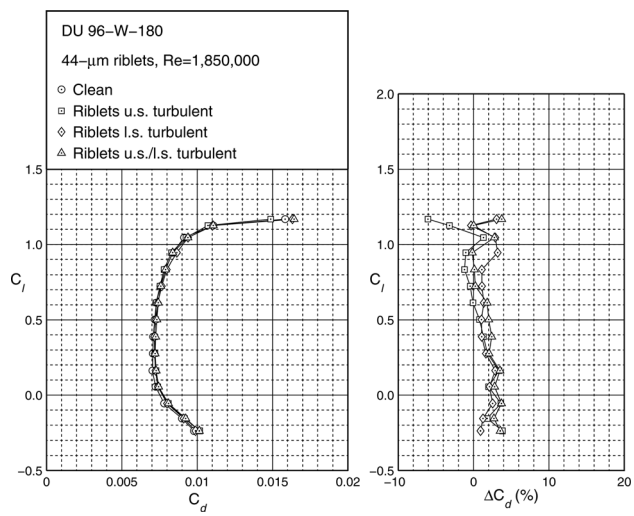

Fig. 16 Drag polar for the DU 96-W-180 at Re = 1,850,000 with 44-μm riblets in the turbulent regions

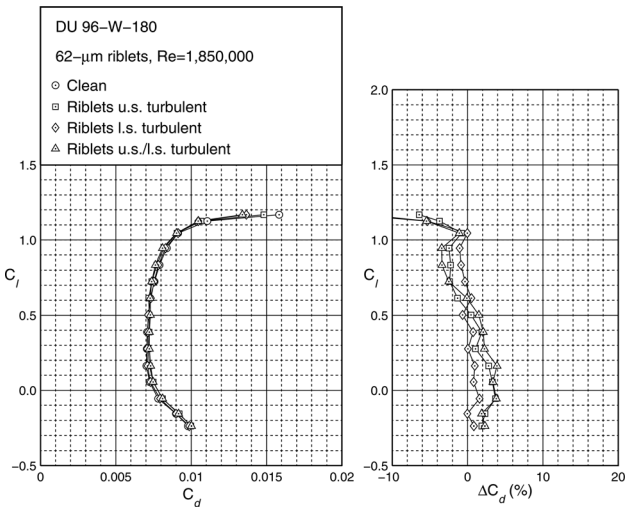

Fig. 17 Drag polar for the DU 96-W-180 at Re = 1,850,000 with 62-μm riblets in the turbulent regions

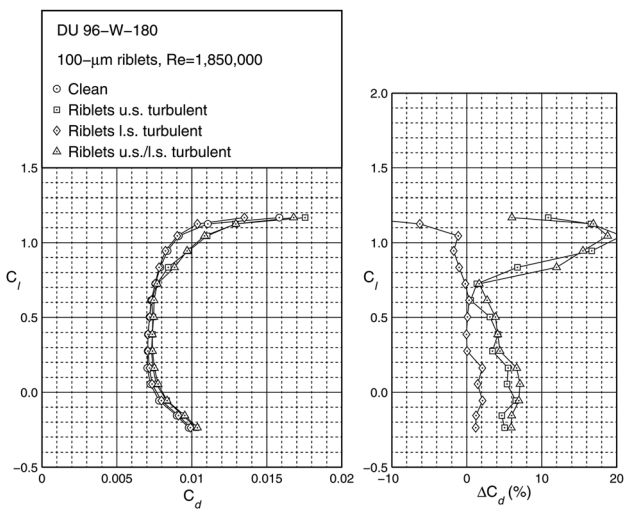

Fig. 18 Drag polar for the DU 96-W-180 at Re = 1,850,000 with 100-μm riblets in the turbulent regions

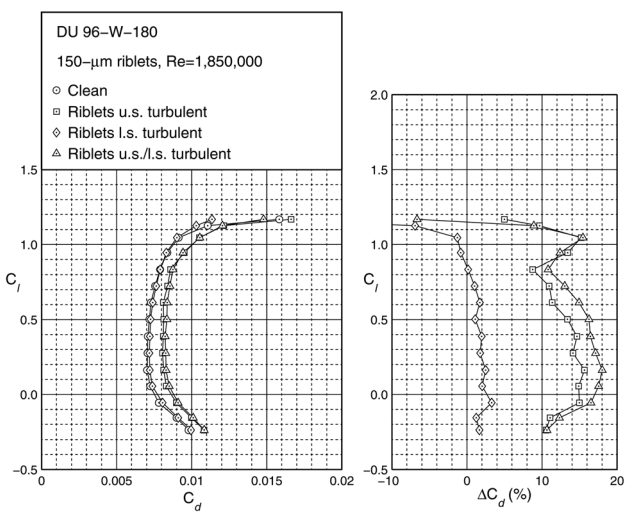

Fig. 19 Drag polar for the DU 96-W-180 at Re = 1,850,000 with 150-μm riblets in the turbulent regions

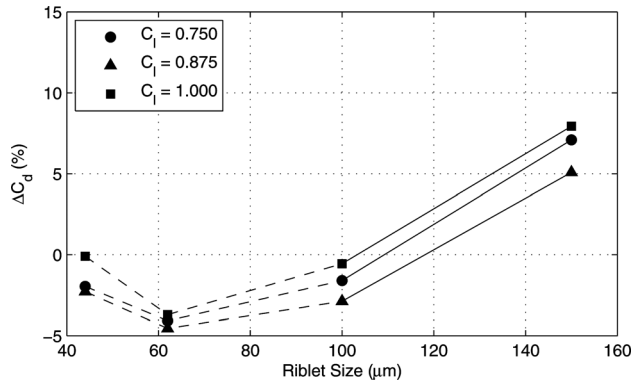

Fig. 20 Percent drag reduction variation with riblet size for the DU 96-W-180 at Re = 1,500,000 and riblets in the upper and lower surface turbulent regions

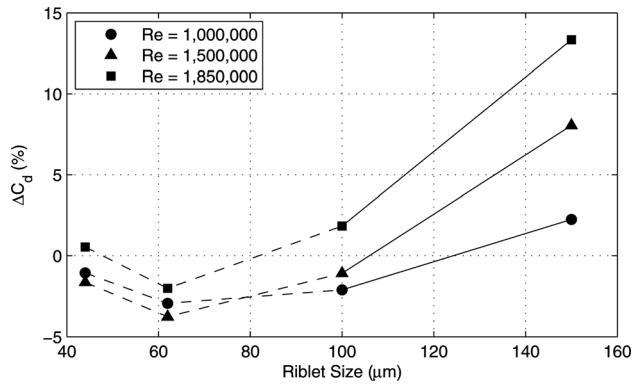

Fig. 21 Percent drag reduction variation with riblet size for the DU 96-W-180 at $C_l = 0.75$ and riblets in the upper and lower surface turbulent regions

4 Conclusions

Various configurations of four different sized riblet films were tested at three Reynolds numbers on the DU 96-W-180 airfoil. Riblets were applied to the turbulent regions of the airfoil to study the changes in the turbulent boundary layer due to riblet action. Results showed that drag reduction due to riblets depends on variables such as the size and location of the riblet film, angle of attack, and Reynolds number. Despite the variables involved, there exists an optimal riblet size that produces maximum drag reduction. For the airfoil and configurations tested, the optimal riblet size was found to be 62 μm. This size was in agreement with theoretical predictions and shows that riblet theory, which is based on a flat plate boundary layer, can be applied to airfoils as well. Optimally sized riblets, when applied in the turbulent region, produced a drag reduction of 4–5%. Nonoptimal riblet sizes, on the other hand, increased drag up to 10–12% in some cases. It was also observed that the Reynolds number at which riblets are most effective decreases as the riblet size increases, which was again, in agreement with riblet theory. Based on results from previous studies on riblets, the performance of riblets is also dependent on the airfoil and hence the optimal riblet size and corresponding drag reduction might be different for other airfoils. The optimal riblet size and performance might also vary for different riblet geometries such as saw toothed and skipped toothed configurations that can be found in literature. In spite of the large variation in riblet performance for the airfoil tested, results showed that it is possible to select a riblet size that performs well over a range of Reynolds numbers and angles of attack. Thus, well-designed airfoils that take advantage of riblet film technology and careful selection of optimally sized riblets based on the knowledge of the operating conditions could potentially enable riblets to be used effectively in real world applications such as wind turbines.

Acknowledgment

The authors wish to thank 3 M Renewable Energy Division (St. Paul, MN) for providing the funding for this research and Dr. G. Memo Izzi and his 3 M technical team for their cooperation that was instrumental in making this study possible. The authors also thank Chris Triphahn for his help with the wind tunnel tests.

Nomenclature

c = airfoil chord
C_d = drag coefficient
C_{fx} = skin friction coefficient
C_m = quarter-chord pitching moment coefficient
C_p = pressure coefficient
C_l = lift coefficient
h = riblet height
$h+$ = nondimensional riblet height
Re = Reynolds number
U_∞ = freestream velocity
x_{tr} = transition location
x/c = normalized chordwise location
α = angle of attack
ν = kinematic viscosity

References

[1] Anonymous, 2005, "Robert L. Ash," Quest, **8**(2), p. 16. Available at http://www.odu.edu/ao/instadv/quest/Ash.html
[2] Walsh, M. J., 1980, "Groves Reduce Aircraft Drag," Technical Brief No. LAE-12599, NASA Langley Research Center.
[3] Walsh, M. J., 1982, "Turbulent Boundary Layer Drag Reduction Using Riblets," AIAA Paper No. 82–0169.
[4] Walsh, M. J., and Lindemann, A. M., 1984, "Optimization and Application of Riblets for Turbulent Drag Reduction," AIAA Paper No. 84-0347.
[5] Walsh, M. J., 1990, "Riblets," *Viscous Drag Reduction in Bounday Layers*, (AIAA Progress in Aeronautics and Astronautics, Vol. 123), D. M. Bushnell and J. N. Hefner, eds., AIAA, Washington, DC, pp. 203–261.
[6] Bechert, D. W., Hoppe, G., and Reiff, W. E., 1985, "On the Drag Reduction of the Shark Skin," AIAA Paper No. 85-0546.
[7] Savill, A. M., 2001, "Riblet Geometries and Wind Turbine Applications and Airbus A330/340 Type Aircraft," Technical Report, Engineering Department, University of Cambridge, Cambridge, UK.
[8] Caram, J. M., and Ahmed, A., 1991, "Effect of Riblets on Turbulence in the Wake of an Airfoil," AIAA J., **29**(11), pp. 1769–1770.
[9] Caram, J. M., and Ahmed, A., 1992, "Development of the Wake of an Airfoil With Riblets," AIAA J., **30**(12), pp. 2817–2818.
[10] Han, M., Lim, H. C., Jang, Y.-G., Lee, S. S., and Lee, S. J., 2003, "Fabrication of a Micro-Riblet Film and Drag Reduction Effects on Curved Objects," The 12th International Conference on Solid State Sensors, Actuators and Microsystems, Vol. 1, pp. 396–399.
[11] Sundaram, S., Viswanath, P. R., and Rudrakumar, S., 1996, "Viscous Drag Reduction Using Riblets on NACA 0012 Airfoil to Moderate Incidence," AIAA J., **34**(4), pp. 676–682.
[12] Raju, C., and Viswanath, P. R., 1998, "Base Drag Reduction Caused by Riblets on a GAW(2) Airfoil," J. Aircraft, **35**(6), pp. 988–991.
[13] Subaschandar, N., Kumar, R., and Sundaram, S., 1999, "Drag Reduction Due to Riblets on a GAW(2) Airfoil," J. Aircraft, **36**(5), pp. 890–892.
[14] Viswanath, P. R., 1999, "Riblets on Airfoil and Wings: A Review," AIAA Paper No. 99-3402.
[15] Viswanath, P. R., and Mukund, R., 1995, "Turbulent Drag Reduction Using Riblets on a Supercritical Airfoil at Transonic Speeds," AIAA J., **33**(5), pp. 945–947.
[16] Wetzel, K. K., and Farokhi, S., 1996, "Interaction of Riblets and Vortex Generators on an Airfoil," AIAA Paper No. 96-2428.
[17] Khodadoust, A., 1993, "An Experimental Study of the Flowfield on a Semispan Rectangular Wing With a Simulated Glaze Ice Accretion," Ph.D. thesis, Department of Aeronautical and Astronautical Engineering, University of Illinois at Urbana-Champaign, Urbana, IL.
[18] Jasinski, W. J., Noe, S. C., Selig, M. S., and Bragg, M. B., 1998, "Wind Turbine Performance Under Icing Conditions," ASME J. Sol. Energy Eng., **120**, pp. 60–65.
[19] Walsh, M. J., 1983, "Riblets as a Viscous Drag Reduction Technique," AIAA J., **21**(4), pp. 485–486.
[20] Drela, M., 1989, "XFOIL: An Analysis and Design System for Low Reynolds Number Airfoils," *Low Reynolds Number Aerodynamics* (Lecture Notes in Engineering, Vol. 54), T. J. Mueller, ed., Springer-Verlag, New York, pp. 1–12.
[21] Timmer, W. A., and van Rooij, R. P. J. O. M., 2003, "Summary of the Delft University Wind Turbine Dedicated Airfoils," ASME J. Sol. Energy Eng., **125**, pp. 488–496.